Probing custerization in ^{40}Ca ^{40}Ca reaction at 35 MeV/A

K. Schmidt, K. Hagel, M. Barbui, S. Wuenschel, G. Giuliani, H. Zheng, E. Kim,
N. Blando, A. Bonasera and J. B. Natowitz

Bose-Einstein condensation is known to occur in weakly and strongly interacting systems such as dilute atomic gases and liquid ^{4}He [1]. During the last decade it was theoretically shown that dilute symmetric nuclear matter may also experience Bose particle condensation [2,3] More precisely, for low temperatures and densities smaller than one fifth of the nuclear saturation density, nuclear matter organizes itself in α-clusters, while for higher densities deuteron condensation is preferred. This possible new phase of nuclear matter may have its analog in low-density states of α-conjugate lighter nuclei, in the same way as superfluid nuclei are the finite-size counterpart of superfluid nuclear and neutron matter. This means that under some circumstances, the alpha condensation, i.e. bosonic properties, might dominate nucleon properties even in finite nuclei [4]. A natural way to pursue this is to apply experimental techniques developed for the investigation of low density nuclear gases to collisions of nuclei expected to have a significant alpha cluster character. Such nuclei might show a more natural predilection to evolve into a Bose Condensate. We have initiated a search for evidence of Bose Condensates using the NIMROD array. Our experiments employed 10, 25, 35 MeV/u beams of ^{40}Ca and ^{40}Si incident on ^{40}Ca, ^{28}Si , ^{12}C and ^{180}Ta targets. The first three targets allow an exploration of collisions of alpha conjugate nuclei. In the ^{180}Ta case the projectile excitation and decay is of primary interest. The data are currently being analyzed. Our expectation is that a Bose Condensate would manifest itself as an assemblage of alpha conjugate products with particular kinematic correlations. Therefore the first step of the analysis was to probe α clusterization in ^{40}Ca + ^{40}Ca at 35MeV/A reaction.

We initiated the analysis of the reaction from reconstructing the excitation energy of each event E* through calorimetry

$$E^* = \sum_{i=1}^{M} K_{cp}(i) + M_n\langle K_n\rangle - Q$$

The excitation energy E* was defined as the sum over accepted particles center of mass kinetic energy (K_{cp} and K_n) minus the reaction Q-value. The average kinetic energy of the neutrons was calculated as the proton average kinetic energy with a correction for Coulomb barrier energy. In Fig. 1 we plot the 3 heaviest fragment masses as a function of parallel velocity in different windows of E*.

Low excitation energies are associated with less violent collisions, therefore in both the experimental data and theoretical calculations we see heavy projectiles (mainly of A=28, 32 and 36 in the experiment) as well as light nuclei. With increasing excitation energy the violence of the collisions increases, we observe a very strong neck-like emission which consists mainly of α like fragments (A=12, 16, 20, 24). Their parallel velocity decreases with the decreasing mass. This has been described in [5] as the "hierarchy effect": the ranking in charge induces on average a ranking in average parallel velocity where the heaviest fragment is the fastest and is more focused in the forward direction.

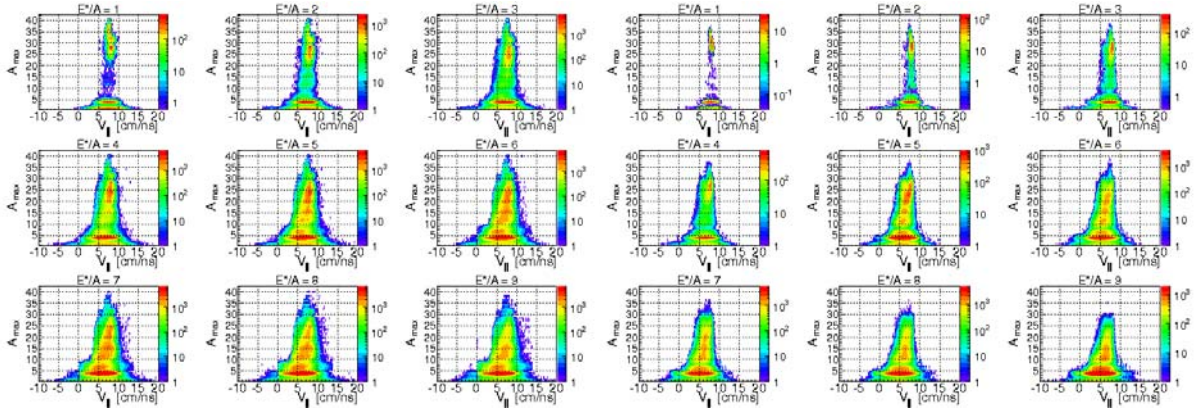

FIG. 1. Three heaviest fragment masses as a function of their parallel velocity in different windows of excitation energy E*/A, left: experimental results, right: theoretical predictions.

Since very strong α clusterization is observed, we attempt to quantify this behavior. In the following we focus on events with α-like mass = 40. 1.3% of experimental events are characterized by α-like mass = 40 whereas the AMD predicts around half that amount, 0.77%. Both experiment and theoretical calculations suggest that the most probable decay modes are those with one heavy α-like mass fragment and several α particles in the exit channel. The contribution of each branch however shows differences between experiment and calculations.

In the experiment the second most probable exit channel is the (^{28}Si, 3α.) Since we are interested in 3α events we focus on this channel. and compare it to (^{28}Si,^{12}C). We show in Fig. 2 the invariant velocity plots of these two decaying branches products. We observe that to a close approximation ^{28}Si moves with the beam velocity (8.21cm/ns) in both cases. The parallel velocity of ^{12}C is consistent with the velocity of the "neck" (see Figure 2) and oscillates around 4-7 cm/ns. Although we observe α particles emerging from the projectile, the majority of them come from a source of intermediate parallel velocity similar to that of ^{12}C. Therefore it will be our priority to focus on the effects related to "neck" emission in further analysis. We will treat it as a separate source of α particles and study its properties.

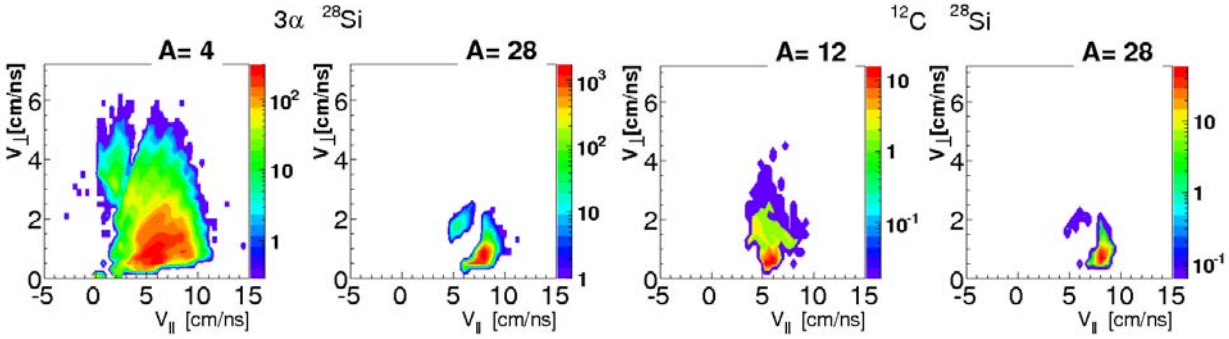

FIG. 2. Invariant velocity plots of 3□+^{28}Si (left) and ^{12}C+^{28}Si (right).

Correlation functions (CF) are defined as the ratio between the correlated (physical) yield Y_{corr} and the product of single particle yields, generically termed as uncorrelated spectrum Y_{uncorr}, measured under the same conditions,

$$1 + R(X) = \frac{Y_{corr}(X)}{Y_{uncorr}(X)}$$

Y_{uncorr} can also be built by mixing particles from different events. Information on the α-particle unstable excited states of ^{12}C populated by the $^{40}Ca+^{40}Ca$ at 35 MeV/nucleon reaction may be extracted from the 3α-CF and Nα-CF. Although 3α-CF is rather intuitive, the Nα-CF requires some explanation. In N-α events there are $\left(\frac{N}{3}\right)$ combinations of such triples of α particles, that could originate from the decay of ^{12}C. We have found all of them and built the E* distribution, which constitues the $Y_{corr}(X)$ in the definition of CF. In order to built the uncorrelated distribution of E* we used α-particles originating from different events. Moreover, we have distinguished between the triples emitted from "neck" and PLF, putting a cut on reconstructed source parallel velocity $V_z \in (4,7)$[cm/ns] for "neck" emission and $V_z \geq 7$[cm/ns] for PLF. In the following figures (Fig. 3 and Fig. 4). we present the CF distributions for alphas originating from neck or PLF, from 3α or Nα events, we compare the experimental data with AMD calculation.

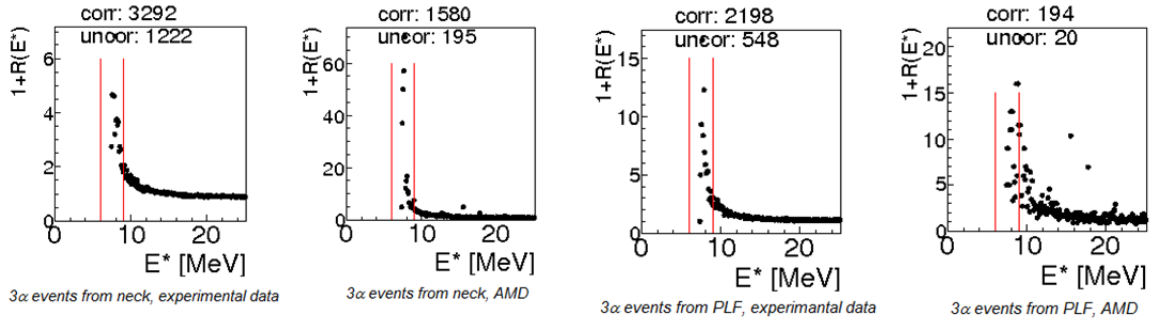

FIG. 3. CF distributions for 3α – events originating from "neck" and PLF, comparison of experimental data and AMD calculations.

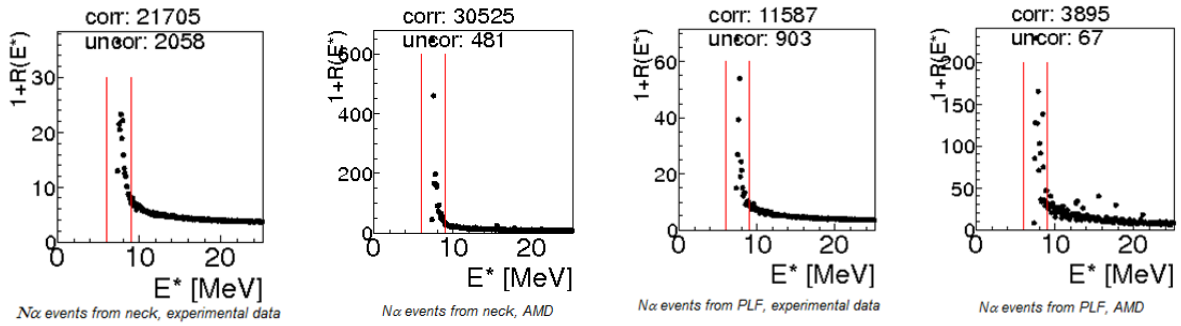

FIG. 4. CF distributions for Nα – events originating from "neck" and PLF, comparison of experimental data and AMD calculations.

All CFs manifest a peak broadening, centered at E*=7.61. It corresponds to the Hoyle state (E^* = 7.654 MeV). Unfortunately the granularity of Nimrod detecting system does not allow us to observe the complex region of excitations, characterized by the strong E* =9.64 MeV, 3^- state and by the broad E* =10.3 MeV, 0^+ state submerging a possible 2^+ state at 9.7 MeV [6,7].

We demonstrated so far that the ^{40}Ca+^{40}Ca nuclear reaction at 35MeV/nucleon populates excited states of ^{12}C nuclei which decay by 3-α emission. We will now examine only those triples, by putting a cut on excitation energy 7≤E*≤9 MeV. A popular way to visualize competing 3-α particle decay mechanisms is the Dalitz plot. In the following pictures we show E_{cm} Dalitz plots for 3α originating from Nα events and from ^{12}C decay, which in turn origins from neck or PLF. The first and the third plot corresponds to experimental data, while the second and the fourth one to AMD simulations. The Dalitz plots (Fig. 5) do not manifest any direct emission in three α-particles with equal energies (DDE) pattern as in [8]. However, the differences in decay mechanism can be noticed, when ^{12}C originates from neck or from PLF. The next step of the analysis will be to explain those differences, provide the theoretical Coulomb trajectories for different shapes of decaying nuclei, examine the shape of experimental decaying nuclei.

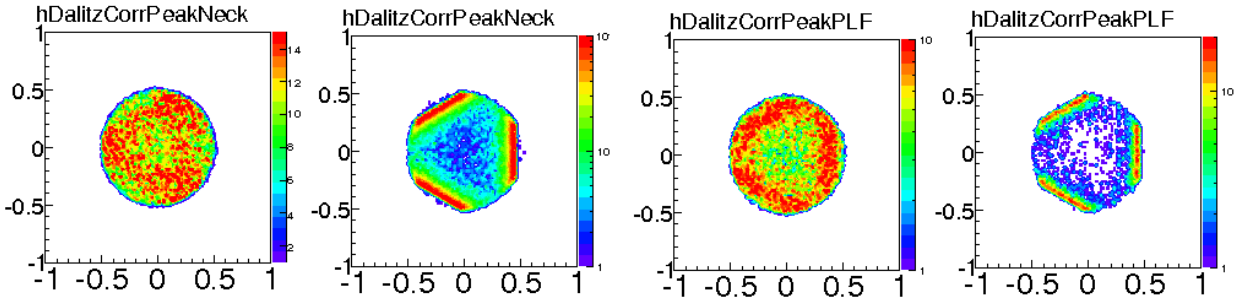

FIG. 5. Dalitz plots for 3-α originating from ^{12}C decay, which in turn originates from neck (the first two plots) and from PLF (the last two plots). Experimantal data are shown in the first and the third plot, AMD calculations in the second and the fourth one.

[1] L.P. Pitaevski and S. Stringari S, Bose-Einstein Condensation, (Clarendon Press, Oxford 2003).

[2] G. Roepke *et al.*, Phys. Rev. Lett. **80**, 3177 (1998).

[3] M. Beyer *et al.*, Phys. Lett. B **448**, 247 (2000).

[4] T. Sogo *et al.*, Phys. Rev. C **79**, 051301 (2009).

[5] J. Colin *et al.*, Phys. Rev. C **67**, 064603 (2003).

[6] M. Itoh *et al.*, Nucl. Phys. **A738**, 268 (2004).

[7] M. Freer *et al.*, Nucl. Phys. **A834**, 621c (2010).

[8] Ad. Raduta *et al.*, Phys. Lett. B **705**, 65 (2011).